

Competing growth mechanisms of Ge/Si(001) coherent clusters

I. Goldfarb, P. T. Hayden, J. H. G. Owen, and G. A. D. Briggs

Department of Materials, University of Oxford, Parks Road, Oxford OX1 3PH, England

(Received 28 March 1997; revised manuscript received 3 July 1997)

The growth of Ge three-dimensional coherent clusters on Si(001) during gas source molecular-beam epitaxy and post-deposition anneals has been investigated using *in situ* elevated-temperature scanning tunneling microscopy. By monitoring the growth of individual so-called ‘‘hut’’ clusters, this technique allowed us to separate various factors that may affect the final size distribution of entire cluster ensembles. It has been found that during the course of epitaxy the hut clusters grow by nucleation and growth of deposited material on the cluster facets; however, the low growth rate ($r \propto t^{1/n}$, where $4 < n < 5$), and the large scatter in absolute rate constants indicate diffusion-limited, rather than interface-limited mass transport, although both the facet-nucleation step and the wetting-layer defects inhibit the cluster growth. The strain-induced energy barriers at the cluster bases prevent material addition, and thus growth of large clusters, facilitating the domination of growth mechanisms other than Ostwald ripening at temperatures below 700 K, leading to symmetric or positively skewed cluster-size distribution functions. The tendency towards negatively skewed and bimodal distributions at higher temperatures signaled the contribution of the ripening in accord with the Lifshitz-Slyozov-Wagner theory. Raising the temperature above 770 K leads to a gradual replacement of the huts by the $\langle 110 \rangle$ -based macroscopic clusters. [S0163-1829(97)05039-X]

I. INTRODUCTION

Because of its growing applicability to a variety of technological applications, heteroepitaxy has become one of the important areas in materials science. The strain introduced in a growing film by the lattice mismatch can be relieved by introduction of defects, such as misfit dislocations, into the epilayer, by roughening the surface of the epilayer, or by a combination of the two. The strain-induced roughening presents a problem in the fabrication of coherently strained electronic devices, which are based on atomically flat layers. However, the two-dimensional (2D) to three-dimensional (3D) transition can be used as a natural way to produce self-assembled devices, in which the carriers are confined to ultrasmall regions (less than the de Broglie electron wavelength) by a potential barrier, such as quantum wires and dots. Unusual electronic and optical properties of quantum dots are described elsewhere and beyond the scope of this work.¹⁻³ Creating those structures by the conventional microlithographic patterning is limited by introduction of irregularities and mechanical damage to the nanostructures. On the other hand, to fully exploit the self-assembling tendency requires an extensive knowledge of growth kinetics and thermodynamics. For either purpose full understanding of the roughening transition during heteroepitaxy is essential.

Ge on Si is a model system for Stranski-Krastanow (SK) growth mode, where the initial 2D wetting layer grows pseudomorphically until the strain due to the 4.2% of lattice mismatch is eventually relaxed via the formation of 3D macroislands.⁴⁻⁶ However, the kinetic route for strain relaxation passes through a series of rather complex surface phase transitions, before reaching the final state of large 3D islands, fully relaxed by dislocations.⁷ One of the particularly important stages of these transitions is the formation of small, fully coherent 3D islands which, because of their small dimensions, can exhibit the electron confinement properties of

quantum dots. These clusters, with their rectangular $\langle 100 \rangle$ -type basis and hutlike shapes formed by $\{501\}$ -type facets, were called ‘‘hut’’ clusters by Mo *et al.*, who were the first to reveal them in their scanning tunneling microscopy (STM) images.⁸ Since then the hut clusters have been identified and characterized by other investigators, using STM,^{9,10} atomic force microscopy (AFM),¹¹ transmission electron microscopy (TEM),⁶ and a variety of diffraction techniques.¹²⁻¹⁴

In a previous work, we have provided a detailed insight into the processes of Ge/Si(001) pit and cluster nucleation, as revealed by *in situ* elevated-temperature scanning tunneling microscopy (ET-STM) during gas-source molecular-beam epitaxy.¹⁵ In this work we describe the next stage, which is further cluster growth in both the mass-nonconserved and mass-conserved regimes. The aim of these experiments was to understand the cluster growth mechanisms and their effect on final cluster densities and size distributions. The two latter quantities are directly related to the application of SK growth to self-assembled quantum dots, via their pronounced effect on the linewidths of photoluminescence spectra.¹⁻³

II. EXPERIMENT

The Si wafers used for this study were *n*-doped 0.1 Ω cm, cut into 1×7 mm² pieces and chemically degreased *ex vacuo*. The samples were handled with ceramic tweezers and clamped to the Ta support on the holder by Ta clamps. In UHV, the samples were degassed for several hours, repeatedly flashed at 1400 K, quenched below 800 K, and slowly cooled to the desired temperature. During the sample flashes and anneals, the pressure was kept below 10^{-7} Pa. Such treatment has generally proved effective in producing well-ordered (2×1) Si surfaces.

A JEOL ET-STM, equipped with low-energy electron diffraction (LEED/Auger) and reflection high-energy electron diffraction (RHEED), and capable of operation up to 1200 $^{\circ}$ C, was used. The base pressure of the STM chamber

prior to growth was 1×10^{-8} Pa. Growth movies were taken during exposure to germane at the growth temperatures and in “constant current” or “Log I” mode, using currents around 0.1 nA and voltages between ± 3 V. Sample heating was achieved by passing direct current through them. Temperatures were measured by optical pyrometer with an accuracy of 30 K. Polycrystalline 0.3-mm W wires were electrochemically etched in 2M NaOH solution to produce atomically sharp tips. GeH₄ (99.99%) was fed through a precision needle valve onto the sample mounted in the STM stage, and the tip was left to scan, while a desired constant pressure was maintained. Two temperatures, 620 and 690 K, and GeH₄ pressures in the 10^{-7} – 10^{-5} Pa range were used for growth. After growth, the samples were annealed at different temperatures, ranging from room temperature (RT) to 800 K, for various periods of time (3–24 h), and imaged using the same STM currents and voltages as in growth movies. RHEED patterns were obtained in the [010] crystallographic direction, using accelerating voltages of 12–15 kV. The cluster coverage was determined by computing the percentage of substrate area covered by clusters.

III. RESULTS

A. Early stage growth

The special type of heterogeneous hut cluster nucleation has been discussed in our previous work.¹⁵ Here, due to our *in situ* capability, we have been able to follow the growth of individual clusters in the early stages. (Throughout this paper we use the same definitions and terminology as in Ref. 16, i.e., in the early stage, the already formed nuclei grow, while the nucleation process continues. The late growth stage starts when the initial supersaturation no longer exists and the nucleation process ceases). As an example, Fig. 1 captures a sequence from the STM movie, in which the nucleation and growth of a typical hut cluster take place. The flat cluster appearance was caused by contrast saturation, since at that point we wished to achieve the best observation conditions of the surrounding wetting layer. At lower contrast values these clusters exhibit perfect {501} facets characteristic of hut clusters.^{7–9,15} Knowing the time interval (54 sec) between sequential scans, we deduced the cluster growth rate. Figure 2 shows an increase in the average cluster size with time for this and three other typical clusters; each reaches the critical nucleus size $r(0)_i$ at a different time $t_{i,0}$. We have defined the average cluster size as the arithmetic mean of both cluster sides (in the [100] and [010] crystallographic directions) in order to be able to compare between clusters with different lateral aspect ratios.

Several important conclusions follow from these observations.

(1) Although the growth rate for some of the clusters is fitted slightly better with an $r \propto t^{1/4}$ dependence (where r is the cluster size), the best fit for most of them, such as those shown here, is achieved with an $r \propto t^{1/5}$ dependence.

(2) The growth is not always continuous, but plateaus, such as those shown in Figs. 2(b) and 2(d), appear occasionally.

(3) Linear fit of the $r(t)_i^5 = r(0)_i^5 + k(t - t_{i,0})$ plots provides two important kinetic parameters, i.e., the critical size

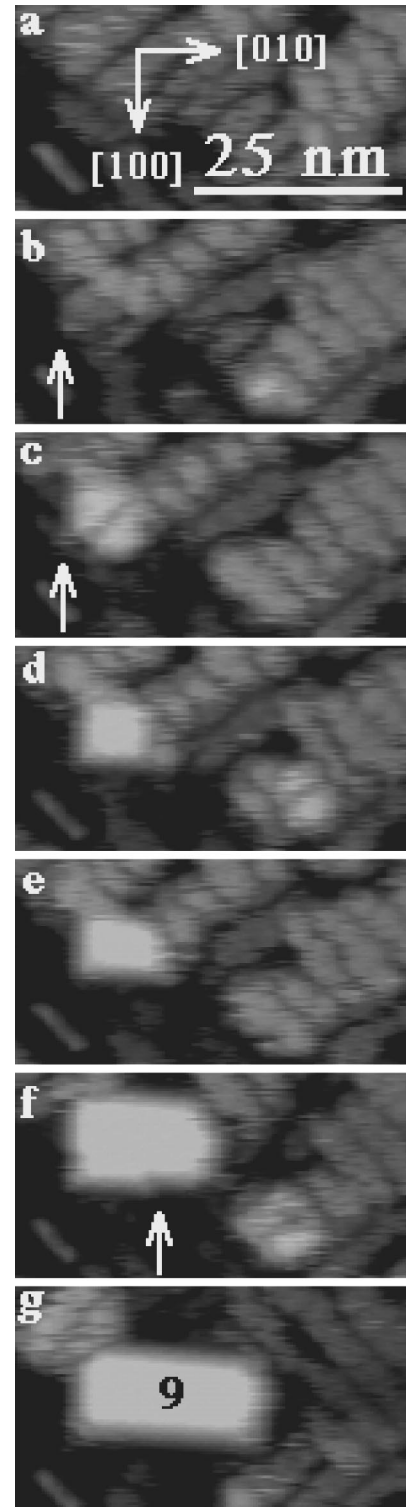


FIG. 1. Nucleation and growth of a typical hut cluster. The arrows point to a formation of the [100] step segment in (b), nucleation at this segment in (c), and advancing front of the pillbox on one of the {501} facets in (f). The flat cluster appearance is caused by high STM contrast value.

for stable nucleation, $r(0)$, and the growth rate constants, k : our best fits for these two parameters yielded $\langle r(0) \rangle = 8 \pm 2$ nm, but the scatter in the rate constant values is much larger; $\langle k \rangle = 695 \pm 244$ nm⁵/sec.

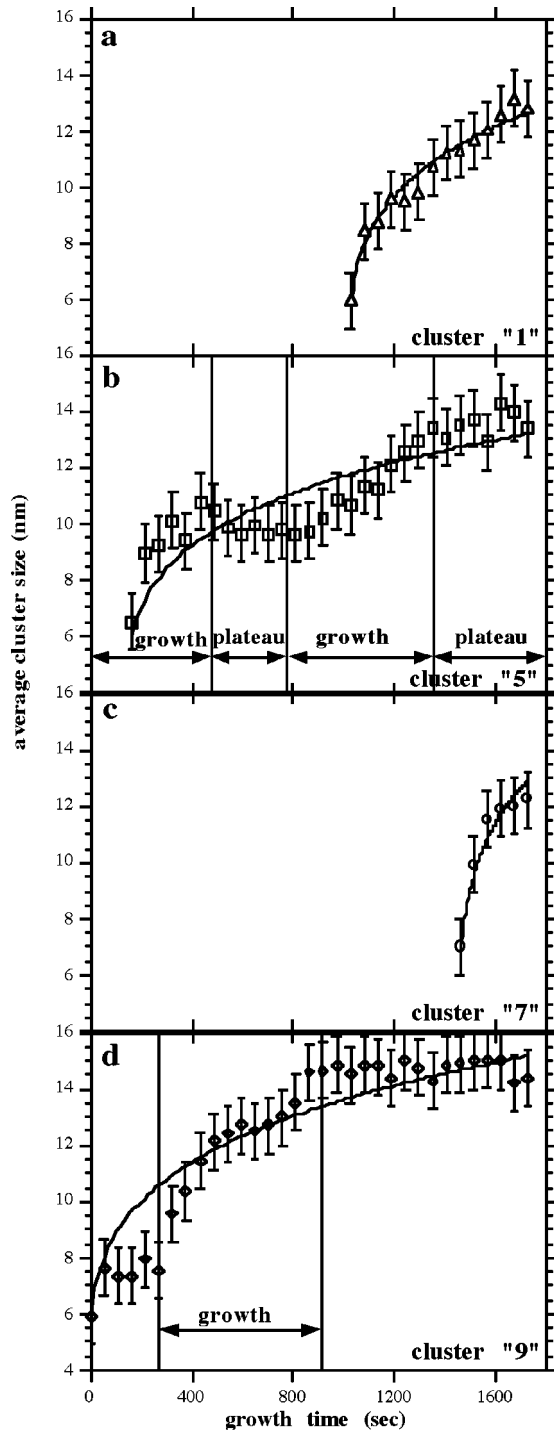


FIG. 2. Typical growth rate curves of hut clusters. The continuous lines represent the best fits for $r \propto t^{1/n}$ ($n=5$), and the bars represent the measurement error.

B. Late stage growth

After the GeH_4 flux was terminated, the samples were subjected to a series of anneals. The first annealing cycle was by cooling the sample from the growth temperature down to RT. The second cycle was to anneal the sample from RT up to 770 K. Figure 3 shows a series of STM images of the Ge grown at 620 K and annealed in the 600–720-K temperature range (combining both heating and cooling cycles), together with the corresponding size distributions. Figure 4 shows a series of STM images of the Ge grown at 690 K and an-

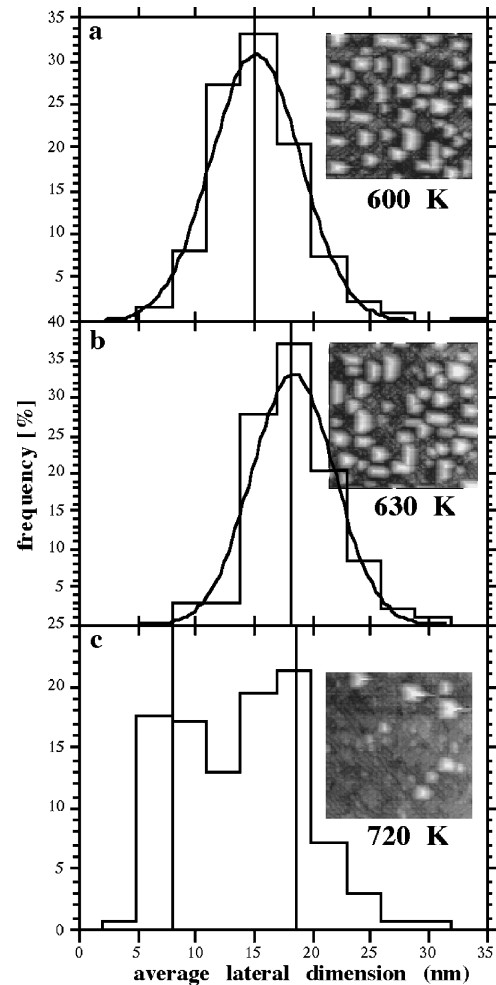


FIG. 3. Typical cluster size distributions after the Ge deposition at 630 K, and subsequent anneals. Note the modality change at 720 K.

nealed in the RT to 670 K temperature range, together with their size distributions. 90 different 40 000-nm² areas and 2800 clusters were statistically analyzed to yield these size distributions. The rather broad symmetrical character of the cluster size distributions is obvious, as well as the increase in mean size with temperature. [Although these distributions are well fitted by Gaussians, their slightly positive skewness values shown in Fig. 6(a) imply that they can also be fitted with log-normal curves.]

IV. DISCUSSION

In this section we present the theoretical models, which are frequently used to treat the clustering phenomena, and show that even when modified, these models are unable to account for the results shown in this work. Therefore, in Sec. V we will propose an alternative model, which qualitatively agrees with these results.

A. General formulations

The late stage growth is driven by the Gibbs-Thomson principle which favors larger sized islands due to the lower vapor pressure around them. Thus smaller islands dissolve to establish concentration gradients towards larger islands,

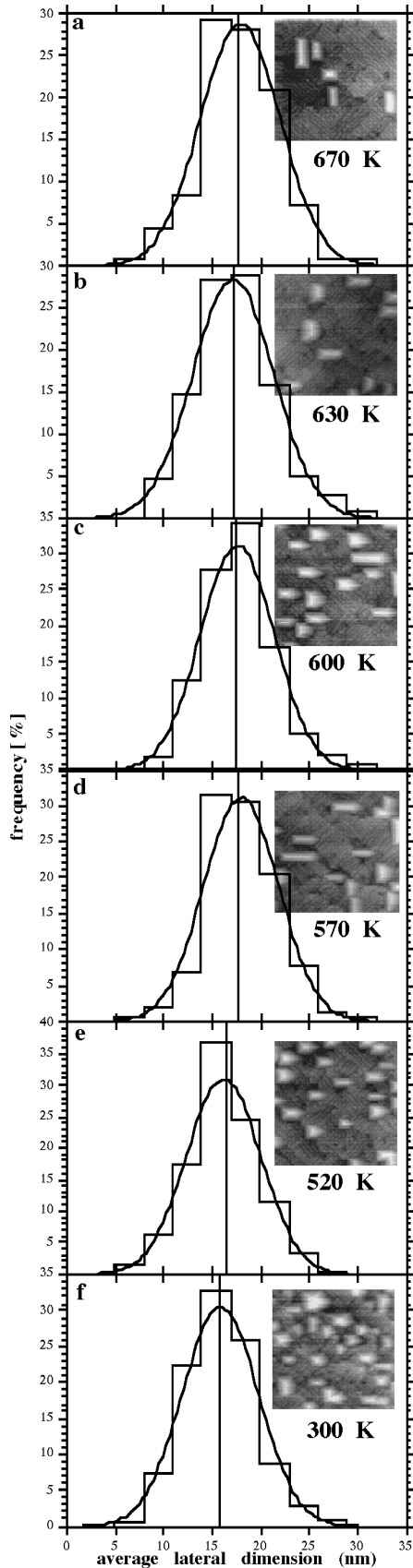


FIG. 4. Typical cluster size distributions after the Ge deposition at 700 K, and subsequent anneals. Note the similarity of the distribution shapes with Fig. 5, in particular for 600 K. Note also the *a priori* higher cluster density in the sample deposited at 630 K.

which continue to grow at the expense of the smaller ones. The first comprehensive theory of this so-called “coarsening” or “ripening” was developed by Lifshitz and Slyozov,¹⁷ extended by Wagner¹⁸ and modified for surfaces by Chakraverty,^{19,20} who also treated the mass-nonconserved and nonzero coverage cases. The Lifshitz-Slyozov-Wagner (LSW) theory, at zero coverage, predicts a universal growth law of the form

$$\frac{dr}{dt} = \frac{\beta(T)}{r^m} \left(\frac{1}{r_c} - \frac{1}{r} \right), \quad (1)$$

where r_c denotes the critical cluster size in equilibrium with the surrounding adatom concentration (i.e., neither grows nor shrinks) and if the deposited material is conserved,

$$r_c(t) = r_c(0) \left(1 + \frac{t}{\tau_c} \right)^{1/(m+2)}, \quad (2)$$

where τ_c is the growth time constant, and the time-independent part of a distribution function depends on m which, in turn, depends upon the dimensionality of the system and the process limiting the mass transport. The use of mass conservation is the factor which restricts the application of the LSW theory to the late growth stages, i.e., when the supersaturation ceases to exist (zero deposition rate). Nevertheless, if there exists a finite supersaturation, which is, however, smaller than the free adatom concentration between the growing clusters, the growth can be described by the Ostwald ripening. The limiting Ge/Si(001) deposition rate has been estimated by Zinke-Allmang *et al.* to be about $5 \times 10^{13} \text{ cm}^{-2} \text{ min}^{-1}$.²¹ Our deposition rates were estimated to be even lower by 2–3 orders of magnitude. Thus in our case even the growth during the deposition stage could be regarded as obeying the LSW conditions. Assumption of a scaling invariance of the distribution function $f(r,t)$ allows to separate it into time-dependent and spatially dependent parts. For the three limiting cases of 3D clusters on the 2D surface, the corresponding time-independent functions $f(\rho)$ have been analytically derived, where ρ is the normalized cluster size $\rho = r/r_c$,^{17–20} and are given below:

$$f(\rho, m=0) = \text{const} \times \rho \left(\frac{2}{2-\rho} \right)^5 \exp \left(-\frac{6}{2-\rho} \right) \quad (\rho \leq 2), \quad (3)$$

for the mass transport limited by the interface transfer with the entire cluster surface active in the process,

$$f(\rho, m=1) = \text{const} \times \rho^2 \left(\frac{3}{3+\rho} \right)^{7/3} \left(-\frac{3/2}{\rho - 3/2} \right)^{11/3} \times \exp \left(\frac{3/2}{\rho - 3/2} \right) \quad (\rho \leq 3/2), \quad (4)$$

when only the boundary line between the cluster and the surface is active, and

$$f(\rho, m=2) = \text{const} \times \rho^3 \frac{\left(\frac{2}{3}\right)^{11/3} \exp\left[-\frac{1}{6\sqrt{2}} \arctan\left(\frac{\rho + \frac{4}{3}}{4\sqrt{\frac{2}{3}}}\right)\right]}{\left(\frac{4}{3} - \rho\right)^{19/6} (\rho^2 + 8\rho + 3 + \frac{16}{3})^{23/12}} \quad (\rho \leq \frac{4}{3}), \quad (5)$$

for the diffusion-limited mass transfer. These functions are characterized by their negative skewness and, apart from the diffusion-limited case, by rather narrow widths at half-maximum (see, for example, Fig. 16 in Ref. 16). The existence of a roughly similar number of clusters with sizes larger and smaller than the average in our distributions, which are well fitted by Gaussian-type curves in Figs. 3 and 4, does not conform to those theoretically predicted functions.

Various experimental systems can deviate from the restrictions imposed by the basic LSW theory. Some of these deviations can change the shape of the size distribution function without changing the growth power law, while others can affect the latter, as well. They can be roughly classified in three categories: the finite volume (coverage in our case) effects, the crystallinity and strain effects, and the nonzero deposition rate effects.¹⁶ In the following sections we will attempt to explain our experimental results by careful application and examination of these concepts.

B. Finite coverage effects

(a) LSW adopted Zener's approximation for the diffusion geometry, assuming large separations between clusters. More realistic approximations, e.g., when the intercluster separations are comparable with cluster sizes, resulted in distribution functions which broaden and become progressively positively skewed.^{16,19,22} In the present case, not only the distribution functions differ from the LSW theory, but as has been deduced from the best fits of the cluster growth rates (see Fig. 2), $m=3$ and lies outside the LSW-predicted values, implying only partial responsibility of the diffusion geometry.

(b) Symmetrical distribution functions described by normal Gaussians,^{23,24} or positively skewed functions described by log-normal curves²⁵ have been attributed to mobility of small clusters on surfaces. Dynamic coalescence of such mobile clusters could explain the presence of clusters with sizes larger than the mean. However we have never observed moving Ge hut clusters, not even the smallest ones. Therefore our results cannot be explained by dynamic coalescence. Static coalescence can also change both the distribution shape and the growth exponent. When two particles touch (encounter), fast diffusive interaction causes the two particles to coalesce and become one, thus removing them from the smaller size ranges of the distribution and adding one to the larger size ranges. This effect is accounted for in the Lifshitz-Slyozov-encounter-modified (LSEM) theory, predicting unimodal but broad and more symmetrical distributions.²² Modifying the approach for 3D clusters on 2D surfaces and constant deposition rates predicts an asymptotic distribution with a power-law decay for small sizes, superimposed on a monodispersed bell-shaped function with its mode at the mean cluster size.²⁶

Excellent agreement with these predictions was observed for the case of Ga/GaAs(001) by Zinke-Allmann, Feldman, and van Saarloos.²⁷ Similar distribution shapes of Ge/Si(001) clusters were observed by Krishnamurthy, Drucker, and Venables who, however, explained them by different growth rates for different size clusters, caused by strain.²⁸

Although it is commonly assumed that coalescence does not play a major role in the late stage regime, e.g., absence of deposition flux,¹⁶ we have observed numerous coalescence events both *in situ* during the early stage growth,¹⁵ and *ex situ* after annealing cycles, i.e., late stage growth. Naturally, coalescence is easily observed *in situ*, as, for example, shown in Fig. 5, which captures the sequence from our growth movie leading to coalescence of two clusters. This type of static coalescence occurs during the early stage growth even at low coverages. One can now understand how problematic it can be to deduce the growth kinetics from size distribution functions alone: compiling the size distribution one would measure the smaller coalesced clusters "10" and "11" as one. Hence, the measured result is the sum of the two. Therefore, when measuring the cluster sizes from our growth experiments, every effort was made to measure each member of the coalesced clusters separately. The probability of coalescence in the late stage regime is proportional to the surface coverage and also increases in the event of cluster bunching, resulting from preferential nucleation at the step edges.¹⁵

C. Crystallinity effects

The misfit strain, which is the very reason for the appearance of Ge/Si clusters, can also significantly alter their growth with respect to the LSW or even LSEM theory. The strain can be released by nucleation of misfit dislocations, but the kinetic barrier for dislocation nucleation increases rapidly with misfit.²⁹ The surface roughness provides a partial strain relaxation by dilatation of lattice planes which are compressed in the 2D film, in spite of the increase in surface energy. In the particular case of Ge/Si(001) hut clusters, x-ray diffraction measurements show the apex region to be almost fully relaxed, while the cluster base is almost fully strained compressively.¹⁴ The strain concentration at the cluster base increases with cluster size, which makes it increasingly difficult for the adatoms to join the cluster.^{30,31} This notion, which has been used to explain narrow cluster size distributions, states that smaller clusters will grow faster than the larger ones, eventually catching up with them,³¹ and therefore completely opposes the ripening concept, where the larger the cluster the faster it grows at the expense of the dissolving smaller ones. This is especially true, i.e., no ripening, for clusters forming a 2D array on the surface.³² When the cluster is large enough for misfit dislocations to be introduced, this loss of coherency removes the obstacle for

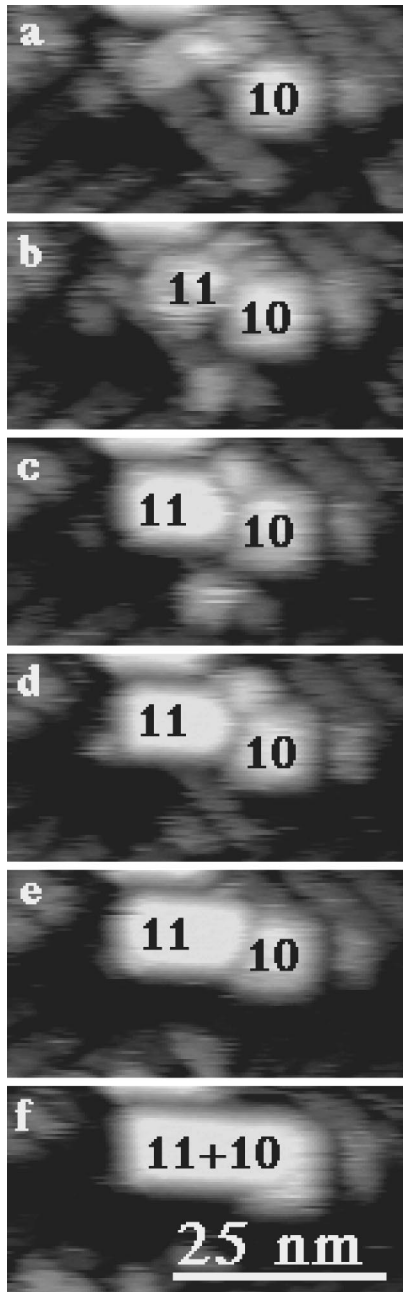


FIG. 5. Typical coalescence event during the early growth stages. (a) Cluster “10” has already nucleated; (b)–(e) however, cluster “11” grows faster than “10,” (f) eventually leading to full coalescence with “10.”

growth, causing acceleration in the cluster’s growth rate, as has been found both experimentally²⁸ and theoretically.³³ Another convincing evidence of the strain effect on ripening comes from applying the opposite reasoning: since in the case of Ge/Si(111) growth the roughening transition does not involve the intermediate small coherent clusters, but directly formed large and incoherent ones, the LSW-type ripening behavior should be expected. This is precisely what has been found, using different experimental methods by Zinke-Allmang *et al.*²² and by Deelman, Thundat, and Schowalter,³⁴ who both found size distributions consistent with the LSW predictions for $m=1$. The striking difference between size distributions for the Ge/Si(001) and Ge/Si(111)

cases obtained within the same experiment is particularly educating.²¹ On the other hand, Gaussian-size distribution functions, rather than the ripening LSW-type functions, are predicted by Priestier and Lannoo when high strain is involved.³⁵

The clusters grow by adatom addition to their {501} facets, as has been proposed by Jesson, Chen, and Pennycook³¹ and experimentally confirmed by Goldfarb *et al.*,¹⁵ as well as by static coalescence.¹⁵ An activation barrier to nucleate a strained facet, which increases with island size and misfit stress,³¹ can be the growth-limiting step. Ahn and co-workers consider such a case of inhibited coarsening of faceted Pt particles on an alumina substrate.³⁶ They found that, while the small particle can shrink according to the simple LSW power law of Eq. (1), the activation barrier for pillbox nucleation on the facet should be entered into the growth rate equation of the growing particle, inhibiting the growth rate. In addition, in the absence of deposition flux, the supersaturation is constantly reduced. The combined effect of the two may manifest itself in growth exponents as low as $\frac{1}{12}$. The resultant size distribution is more positively skewed than the one expected from the LSW treatment. Such an inhibited-growth model is in qualitative agreement with our results. It is worthwhile to note that in the diffusion-limited cases, a reduction of the growth exponent can also be expected, if the diffusion is limited to certain paths, instead of the entire intercluster area. Any additional limitation will further reduce the growth exponent, which again is consistent with $m=3$ deduced from our *in situ* experiments. However, as has been shown by Vegrenovitch,³⁷ this will, in turn, lead to even more negatively skewed and narrower distribution functions. Ultimately, when m is sufficiently large, the interval of relative size variation will tend to unity, in complete agreement with the δ -functional LSW behavior, in disagreement with our size distributions, as can be judged from Figs. 3(a), 3(b), and 4. [Figure 3(c) is a special case and will be discussed separately.]

D. Nonzero deposition rates

As was stated previously, in view of the low deposition rates used in our experiments, we believe they are well approximated by the LSW assumption of zero deposition rate. However, it is interesting to compare the Ge clusters growth exponent of 0.2 from our measurements, to 0.23 measured for water droplets on glass, after separating the coalescence events in the mass-nonconserved regime.³⁸ The authors also explained this low exponent by the absence of ripening.

V. THE MODEL

Simple coarsening, during which larger clusters grow at the expense of smaller ones, is clearly inapplicable in our case, since those larger clusters are progressively prevented from growing further by the large compressive strain at their bases, as manifested through the consistently positive skewness of cluster size distribution functions shown in Fig. 6(a). Coverage independence of both the standard deviation and skewness in Fig. 6, as well as the decrease of cluster coverage with increasing temperature seem to exclude the finite coverage effects, which could have otherwise explained broad and positively skewed cluster distributions by diffu-

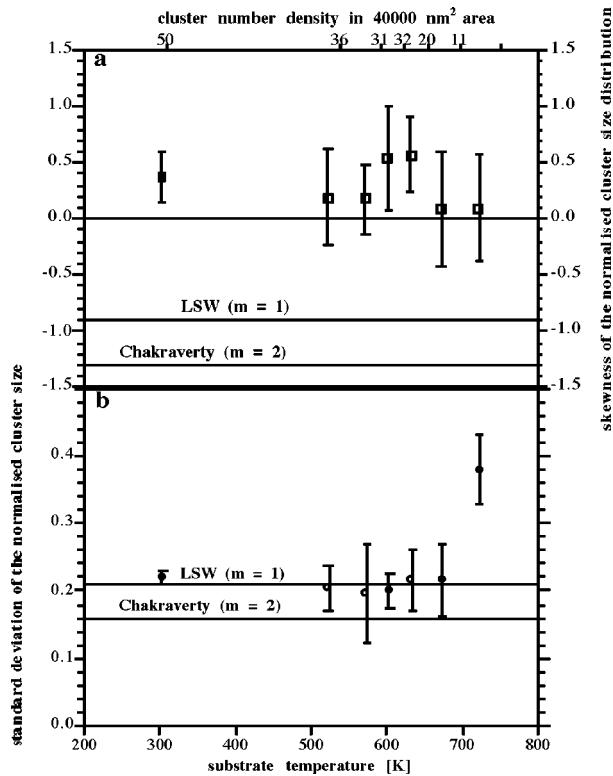


FIG. 6. Temperature (lower abscissa) dependence of the (a) cluster size standard deviation and (b) skewness. The bars stand for standard deviations of the values. The upper abscissa shows the cluster number density values for each temperature. The decrease of cluster density with temperature is apparent. The LSW-Chakraverty values for $m=1$ and 2 are given for comparison. Note the sudden increase in the value of standard deviation at 720 K (indicative of the modality change) relative to a rather constant behavior up to 720 K, as well as consistently positive skewness values.

sive interaction between neighboring clusters and increased coalescence probability.³⁹ Furthermore, although reduction of cluster number density with increasing temperature is to be expected in coarsening- or coalescence-dominated growth, in the mass-conserved regime the area covered by the clusters should be temperature independent, contrary to the linear proportionality between the area covered by clusters and their number density, shown in Fig. 7. Finally, it could be argued that the distribution shapes observed by us could result from interface-controlled coarsening, where the

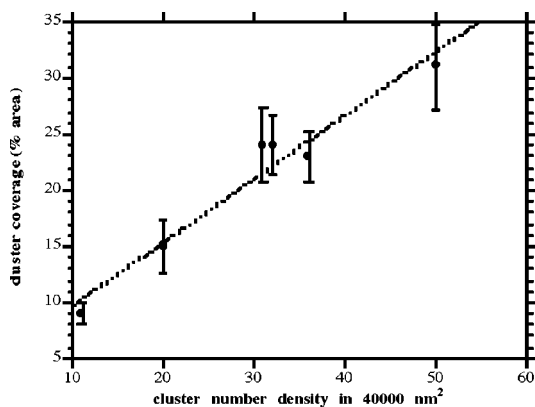


FIG. 7. Cluster areal coverage dependence on cluster density.

whole cluster surface is active in the mass transport ($m=0$). However, such a growth mechanism would imply the linear dependence of cluster size with time, i.e., growth exponent of 1, as opposed to the 0.2 growth exponent found by us. The probable reason is the low cluster sticking coefficient, as was experimentally observed by us, implying mass transport of the deposited material from the wetting layer to the clusters, rather than directly from the vapor phase. This indicates gradual material “climb” from the cluster base upwards, contrary to the concept of full cluster surface activity. On the other hand, the inhibited coarsening model for faceted particles, proposed by Ahn and co-workers³⁶ (see Sec. IV), although consistent with the low-value of growth exponents, is inconsistent neither with the simple power law observed by us during deposition, nor with the large scatter of the absolute growth rate constants. It seems that if a certain part of our results can be accounted for using one or more of the existing models, the rest of the results are in contradiction. Therefore, we would like to propose a model for the growth of Ge clusters on Si(001) surfaces, based on redistribution of the material released from the shrinking clusters. We will show that, at least up to 700 K, neither coarsening nor coalescence dominate the growth.

At the early stages of growth the main activation barrier is the diffusion barrier, as can be judged from the large scatter of the growth rate constants, with the successive nucleation barrier seen as plateau in the cluster growth curves. At the late growth stages, due to the Gibbs-Thomson effect, the smaller the cluster the less stable it is. At each temperature a threshold value of cluster size can be defined, below which the probability of a cluster to survive is very low. However the material released from these decomposing clusters will be transferred back to the intercluster wetting layer, because the larger ones are “locked” by the energy barrier at their bases. The wetting layer, on the other hand, cannot grow further because it has already exceeded the critical thickness. Thus the material released is redistributed to agglomerate and form fewer clusters but with sizes larger than the threshold value. Such a “redistribution” process involving the wetting layer will yield positively skewed distribution functions, reduction of the cluster number density as well as the cluster areal coverage, and shift to higher mean-size values with increasing temperature. This is in qualitative agreement to our results. Note also that this process can be alternatively described by the coalescence of those small clusters, but if this is the case, the larger clusters should coalesce as well, producing clusters in the largest size range of the distribution function, contrary to the observed.

This mechanism seems to prevail in the temperature range from RT up to 700 K. At higher temperatures, for example, at 720 K, the bimodal cluster distribution shown in Fig. 3(c) indicates a contribution from a different growth mechanism. At this temperature, the adatoms have more thermal activation and increased probability to join the larger clusters. In other words, the coarsening is also allowed to take place, while the redistribution is still going on. Those two simultaneous processes are the reason for the bimodal character of the cluster distribution in Fig. 3(c). Due to inhomogeneities of the wetting layer, there can be found regions in which the redistribution process prevails, and regions dominated by coarsening. Figure 8 shows two different sample regions at

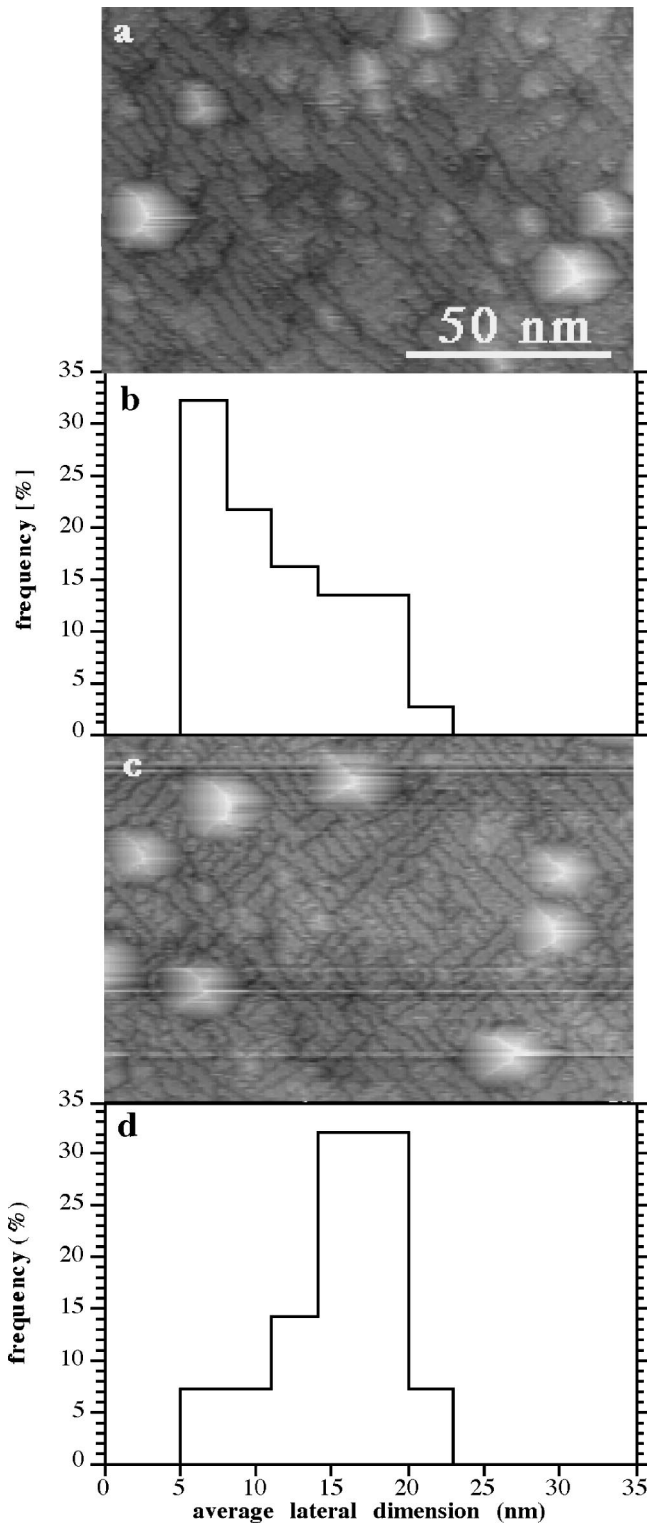


FIG. 8. Typical sample regions at 720 K. (a) “Redistribution”-type region with its (b) characteristic cluster distribution, and (c) “coarsening”-type region with its (d) cluster distribution.

720 K and their corresponding distribution functions. Figure 8(a) is characterized by the majority of small clusters in various stages of dissolution and redistribution, which, therefore continuously cover a wide range of small sizes, with fewer large clusters in the distribution tail. The resultant strongly positively skewed distribution shown in Fig. 8(b) is indicative of the dominating redistribution process. Figures 8(c)

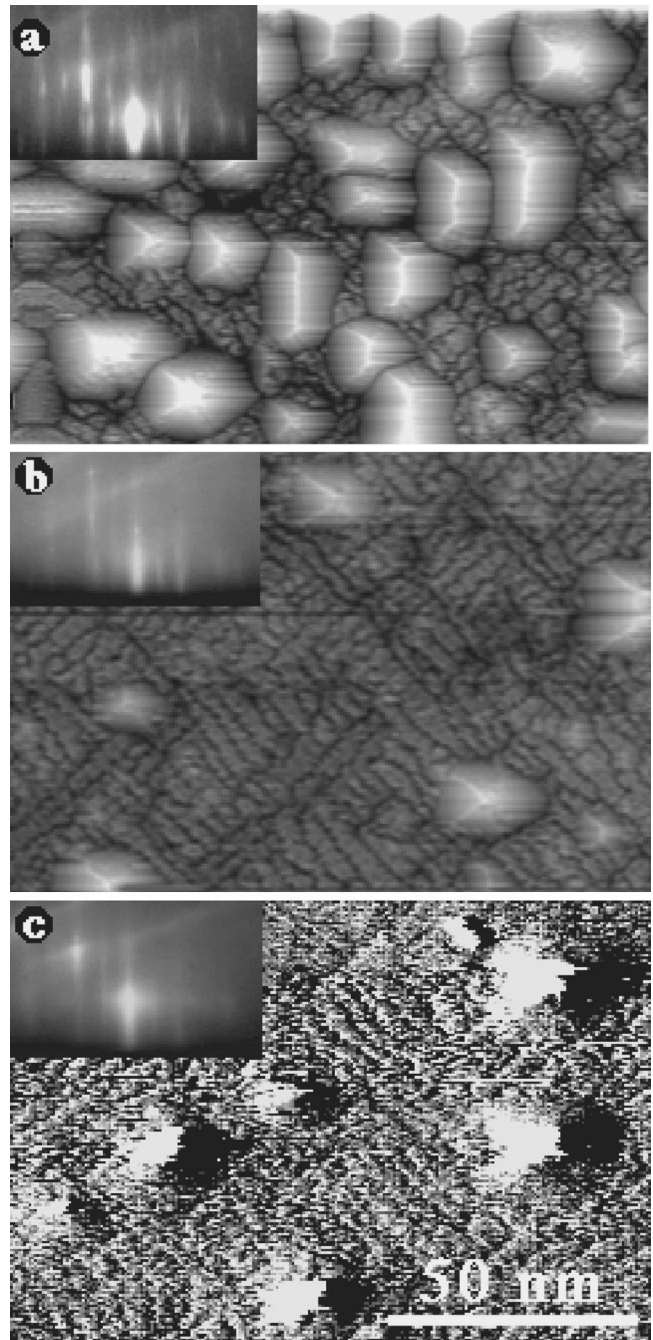


FIG. 9. Hut cluster evolution with temperature. Note the sharp and intense split lines in the inset of (a), diffuse nature of split lines in the inset of (b), and the no longer faceted cluster appearance in (c) with the corresponding absence of splitting in the inset. The STM image in (c) is taken in the “Log I” mode.

and 8(d) exhibit a cluster distribution which is strongly skewed towards the larger cluster size (negative skewness), and thus characteristic of coarsening. Superposition of these two produces the two humps in the distribution function of Fig. 3(c).

Raising the temperature to even higher values leads to replacement of the metastable huts by large incoherent clusters. The replacement occurs in stages. Figure 9 shows a series of STM images characteristic of the hut cluster evolution, and Fig. 10 shows a plausible pattern of the macroscopic cluster formation. At annealing temperatures T

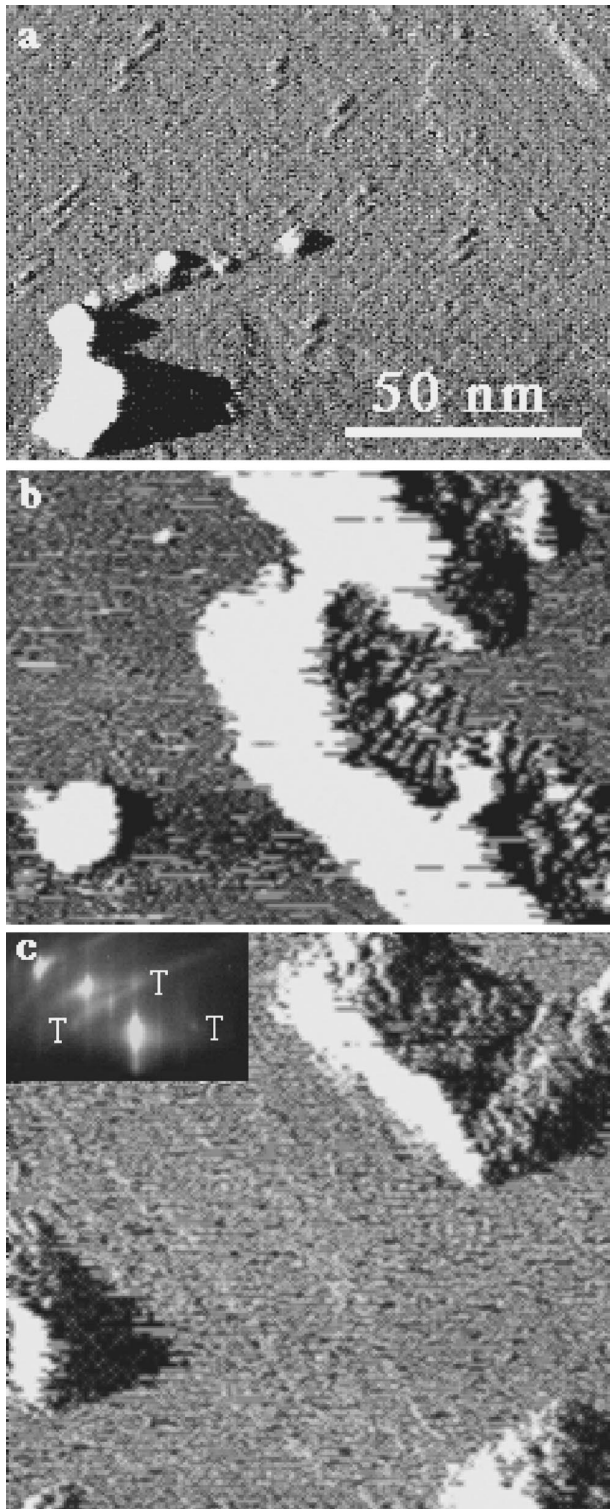


FIG. 10. “Log I” STM images describing the proposed mechanism of the macrocluster formation. (a) The material from the dissolving microclusters is deposited back onto the wetting layer in a form of dimer strings, as well as transferred to the step edges (note the “tailing” of the material from the dissolving microcluster towards the nearest step). (b) The resulting thickening of the step edges and, finally (c) formation of the macroclusters. Note the $\langle 110 \rangle$ -oriented macrocluster bases parallel to steps, as well as transmission spots (marked “T”) in the RHEED pattern, characteristic of the bulk nature of the macroclusters.

< 670 K the surface is characterized by a rather dense and unimodal distribution of well-defined huts, resulting in the intense 11° -split $[010]$ RHEED pattern. Typical constant-current STM image of such a surface is shown in Fig. 9(a), with the corresponding RHEED pattern in the inset. Typical STM and RHEED patterns for the $670 \leq T < 770$ K annealing regime are shown in Fig. 9(b). The smeared and weak-split diffraction lines reflect reduction in the number of the large clusters and smeared distribution of the smaller ones. These stages of cluster evolution have been discussed so far. During the next stage ($T \geq 770$ K) the huts lose their facets and become conically shaped, as can be seen in the “Log I” STM image in Fig. 9(c). Facet disappearance is immediately manifested in the no longer split RHEED lines, in the inset of Fig. 9(c). Then even the largest clusters begin to dissolve, and material from those dissolved clusters is again transferred onto the intercluster wetting layer. However at this point, probably due to the loss of coherency and the resulting relaxation, the wetting layer is able to absorb the additional material [Fig. 10(a)]. It is striking to see this additional material take the form of the (2×1) dimer strings, just as during the initial stages of Ge deposition onto the still unstrained Si(001) surface.⁴⁰ When a dissolving cluster is in the vicinity of a step, the material released is preferentially adsorbed at the step edge, as may be deduced from Fig. 10(a) by the material “tail” from such a cluster to a step. This “tail” is also indicative of the mobility of small clusters at such a high temperature. This results in a thickening of such a step [Fig. 10(b)] and, finally, a formation of macroscopic clusters with their bases parallel to steps [Fig. 10(c)]. The bulk nature of those macroclusters is evident from the transmission spots, arrowed in the RHEED pattern in the inset. A process of this kind can also explain the $\langle 110 \rangle$ -type bases of the macroclusters, which remained unclear so far, although some explanations have been proposed.⁷ At this point we cannot account for the absence of the $\{113\}$ facets from these clusters,^{7,41} but it seems that at these temperatures the steps are more favorable than the facets or, alternatively, that due to the activated nature of facet formation perhaps higher-temperature anneals are required for those facets to develop.

VI. CONCLUSIONS

In our previous work we have explained mechanisms of nucleation of Ge/Si(001) hut pits and clusters. In this work, which is the natural extension of the previous one, we describe the complex and competing growth mechanisms of the hut clusters in various growth regimes.

In the early growth stage, the clusters grow by an addition of the deposited material from the intercluster wetting layer, onto their $\{501\}$ facets. While the clusters are still small the activation barrier for pillbox nucleation on the facet is not sufficiently high, and the growth is limited by surface diffusion, as follows from the low growth exponent and the large scatter of absolute rate constants of the growing clusters.

Although the late stages of growth are usually attributed to Ostwald ripening, in this case the large clusters are prevented from ripening by an activation barrier for the nucleation of a strained facet. Hence, although the smaller clusters obey the Gibbs-Thomson principle and dissolve, at $T < 720$ K the released material reaggglomerates on the wetting

layer to form a lesser number of however larger clusters, instead of being used to coarsen the existing larger clusters. Such a "material redistribution" process results in positively skewed unimodal cluster size distributions, with a mean value slowly shifted towards higher sizes with increasing temperature. The finite coverage effects, such as diffusive interactions between neighboring clusters, do not seem to play a major role in the growth, as concluded by analyzing coverage dependence of the higher moments of the distribution function. More direct coverage effects, such as the static cluster coalescence, have been witnessed to occur at early, as well as late stages of growth.

When the temperature is raised to about 720 K, the adatoms are sufficiently activated to begin to overcome the energy barrier surrounding the large-sized clusters, and the

resulting bimodal size distribution reflects contributions from the both redistribution and ripening processes. If the temperature is allowed to rise above 770 K, the metastability limit of hut clusters is exceeded and they begin to disappear from the surface, initially by losing their facets and attaining conical shapes, and finally by transferring their material back to the wetting layer and to the step edges. The resulting thickening of the step edges leads to a formation of macroscopic clusters with their bases oriented parallel to steps.

ACKNOWLEDGMENT

This work was supported by Engineering and Physical Sciences Research Council (EPSRC) (GR/K08161).

-
- ¹L. Banyai and S. W. Koch, *Semiconductor Quantum Dots* (World Scientific, Singapore, 1993).
- ²R. Nötzel, *Semicond. Sci. Technol.* **11**, 1365 (1996).
- ³P. M. Petroff and G. Medeiros-Ribeiro, *MRS Bull.* **21**, 50 (1996).
- ⁴D. J. Eaglesham and M. Cerullo, *Phys. Rev. Lett.* **64**, 1943 (1990).
- ⁵D. J. Eaglesham and M. Cerullo, *Mater. Sci. Eng. B* **30**, 197 (1995).
- ⁶M. Hammar *et al.*, *Surf. Sci.* **349**, 129 (1995).
- ⁷M. Tomitori *et al.*, *Appl. Surf. Sci.* **76/77**, 323 (1994).
- ⁸Y.-W. Mo *et al.*, *Phys. Rev. Lett.* **65**, 1020 (1990).
- ⁹J. Knall and J. B. Pethica, *Surf. Sci.* **265**, 156 (1991).
- ¹⁰M. Tomitori *et al.*, *Surf. Sci.* **301**, 214 (1994).
- ¹¹D. E. Jesson *et al.*, *Phys. Rev. Lett.* **77**, 1330 (1996).
- ¹²C. E. Aumann, Y.-W. Mo, and M. G. Lagally, *Appl. Phys. Lett.* **59**, 1061 (1993).
- ¹³N. Ohshima *et al.*, *Appl. Phys. Lett.* **63**, 3055 (1993).
- ¹⁴A. J. Steinfort *et al.*, *Phys. Rev. Lett.* **77**, 2009 (1996).
- ¹⁵I. Goldfarb *et al.*, *Phys. Rev. Lett.* **78**, 3959 (1997).
- ¹⁶M. Zinke-Allmang, L. C. Feldman, and M. H. Grabow, *Surf. Sci. Rep.* **16**, 377 (1992).
- ¹⁷I. M. Lifshitz and V. V. Slyozov, *J. Phys. Chem. Solids* **19**, 35 (1961).
- ¹⁸C. Wagner, *Z. Elektrochem.* **65**, 581 (1961).
- ¹⁹B. K. Chakraverty, *J. Phys. Chem. Solids* **28**, 2401 (1967).
- ²⁰B. K. Chakraverty, *J. Phys. Chem. Solids* **28**, 2413 (1967).
- ²¹M. Zinke-Allmang *et al.*, *Phys. Rev. B* **39**, 7848 (1989).
- ²²C. S. Jayanth and P. Nash, *J. Mater. Sci.* **24**, 3041 (1989).
- ²³K. Heineman and H. Poppa, *Thin Solid Films* **33**, 237 (1976).
- ²⁴M. Listvan, *Surf. Sci.* **173**, 294 (1986).
- ²⁵R. Vincent, *Proc. R. Soc. London, Ser. A* **321**, 53 (1971).
- ²⁶F. Family and P. Meakin, *Phys. Rev. Lett.* **61**, 428 (1988).
- ²⁷M. Zinke-Allmang, L. C. Feldman, and W. van Saarloos, *Phys. Rev. Lett.* **68**, 2358 (1992).
- ²⁸M. Krishnamurthy, J. S. Drucker, and J. A. Venables, *J. Appl. Phys.* **69**, 6461 (1991).
- ²⁹J. Tersoff and R. M. Tromp, *Phys. Rev. Lett.* **70**, 2782 (1993).
- ³⁰Y. Chen and J. Washburn, *Phys. Rev. Lett.* **77**, 4046 (1996).
- ³¹D. E. Jesson, K. M. Chen, and S. J. Pennycook, *MRS Bull.* **21**, 31 (1996).
- ³²V. A. Shchukin *et al.*, *Phys. Rev. Lett.* **75**, 2968 (1995).
- ³³J. Drucker, *Phys. Rev. B* **48**, 18 203 (1993).
- ³⁴P. W. Deelman, T. Thundat, and L. J. Schowalter, *Appl. Surf. Sci.* **104/105**, 510 (1996).
- ³⁵C. Priester and M. Lannoo, *Phys. Rev. Lett.* **75**, 93 (1995).
- ³⁶T.-M. Ahn and J. K. Tien, *J. Phys. Chem. Solids* **37**, 771 (1976); T.-M. Ahn, S. Purushothaman, and J. K. Tien, *ibid.* **37**, 777 (1976).
- ³⁷R. D. Vegrenovitch, *Acta Metall.* **30**, 1079 (1982).
- ³⁸D. Beysens and C. M. Knobler, *Phys. Rev. Lett.* **57**, 1433 (1986).
- ³⁹R. Barel *et al.*, *Appl. Surf. Sci.* **104/105**, 669 (1996).
- ⁴⁰Y. W. Mo and M. G. Lagally, *Surf. Sci.* **248**, 313 (1991).
- ⁴¹F. Tuinstra *et al.*, *Surf. Sci.* **317**, 58 (1994).